Computer Aided Geometric Design 85 (2021) 101975

Contents lists available at ScienceDirect

Computer Aided Geometric Design

www.elsevier.com/locate/cagd

27 variants of Tutte's theorem for plane near-triangulations and an application to periodic spline surface fitting

Lisa Groiss [a], Bert Jüttler [a,*], Dominik Mokriš [b]

[a] Institute of Applied Geometry, Johannes Kepler University, Linz, Austria
[b] MTU Aero Engines AG, Munich, Germany

ARTICLE INFO

Article history:
Available online 16 March 2021

Keywords:
Tuttes's theorem
Mesh parameterization
Floater's parameterization
Plane near-triangulation

ABSTRACT

The theoretical basis of Floater's parameterization technique for triangulated surfaces is simultaneously a generalization (to non-barycentric weights) and a specialization (to a plane near-triangulation, which is an embedding of a planar graph with the property that all bounded faces are – possibly curved – triangles) of Tutte's Spring Embedding Theorem. Extensions of this technique cover surfaces with holes and periodic surfaces. The proofs presented previously need advanced concepts, such as rather involved results from graph theory or the theory of discrete 1-forms and consistent perturbations, or are not directly applicable to the above-mentioned extensions. We present a particularly simple geometric derivation of Tutte's theorem for plane near-triangulations and various extensions thereof, using solely the Euler formula for planar graphs. In particular, we include the case of meshes possessing a cylindrical topology – which has not yet been addressed explicitly but possesses important applications to periodic spline surface fitting – and we correct a minor inaccuracy in a previous result concerning Floater-type parameterizations for genus-1 meshes.

1. Introduction

In a seminal paper, Floater (1997) introduced a powerful parameterization method for triangulated surfaces patches based on graph theory. For given parameter values of the boundary vertices, the parameterization of the inner vertices is generated via convex combinations, resulting in a system of linear equations. Special attention has been paid to the choice of the convex combination weights, in order to obtain visually smooth results in the subsequent surface approximation step (Floater and Hormann, 2005). Floater's parameterization method is a fundamental building block of various techniques for surface reconstruction (Weiss et al., 2002; Vaitkus and Várady, 2018; Bracco et al., 2018). In addition, it triggered a substantial amount of research on generalized barycentric coordinates (see, e.g., Jiang et al., 2020; Deng et al., 2020). Generalizations to more general surface topologies have also been investigated (Gotsman et al., 2003; Aigerman and Lipman, 2015; Campen et al., 2019).

The theoretical foundation for this method dates back to Tutte (1963), who analyzed realizations (embeddings into the plane) of planar graphs via convex combinations. Tutte's proof applies to a fairly general class of graphs (nodally 3-connected planar graphs) that may have non-triangular faces, and it makes use of rather involved results from graph theory.

* Corresponding author.
E-mail addresses: lisa.groiss@jku.at (L. Groiss), bert.juettler@jku.at (B. Jüttler), dominik.mokris@mtu.de (D. Mokriš).

https://doi.org/10.1016/j.cagd.2021.101975

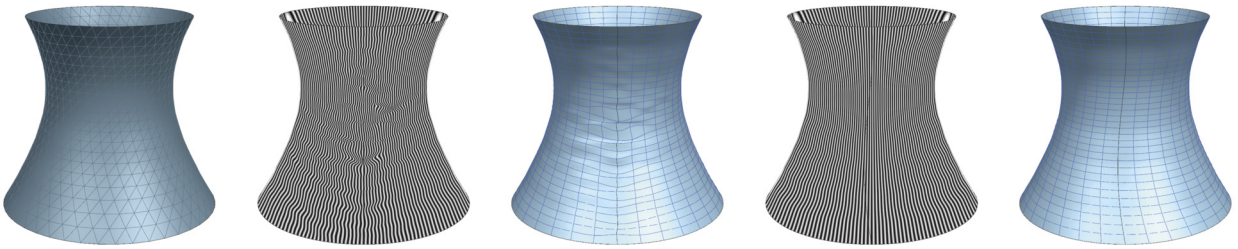

Fig. 1. Periodic spline surfaces generated by fitting triangulated data from a hyperboloid of one sheet. From left to right: the input triangulation; reflection lines and knot lines using a non-periodic Floater parameterization; reflection lines and knot lines using a periodic Floater parameterization.

A book of Richter-Gebert (1996) includes another graph-theoretical proof of Tutte's theorem, which is less opaque than the original one. Besides using graph-theoretic arguments, he employs an intuitive geometric argument (based on the angle excess around a vertex) and uses perturbations to exclude degenerate situations.

Floater (2003) proves a specialization – which can be seen as a discrete version of the Radó-Kneser-Choquet theorem – of Tutte's result to triangulations,[1] i.e., to embeddings of planar graphs with the property that all bounded faces are triangles (with straight edges). He also derives improvements of it, by relaxing the assumptions regarding the strict convexity of the boundary and the property of 3-connectedness. The extension of these results to more general tilings of the plane was presented in a follow-up paper (Floater and Pham-Trong, 2006).

The significant progress made in the theory of discrete one-forms (Gu and Yau, 2003) was exploited by Gortler et al. (2006) to establish another proof of Tutte's theorem for 3-connected planar graphs. In addition, these authors succeeded to derive various generalizations, to meshes with multiple boundaries and to meshes with genus 1 (which are topologically equivalent to the torus). Among the various proofs of different versions of Tutte's theorem, which were used in the above-mentioned and other earlier publications, the techniques used by Gortler et al. (2006) appear to be much more accessible to an audience without expert knowledge in graph theory. Still, rather technical perturbation arguments are needed to rule out degeneracies.

Our interest in this topic was triggered by the application of Floater's method to periodic spline surfaces, in particular for the reconstruction of turbine blades from triangulated laser scan data. It became soon obvious (and is demonstrated by the simple academic example in Fig. 1) that the application of the standard version of Floater's method to a mesh with a cylindrical topology that is cut open by an auxiliary surface does not give good results. Though the extension of Floater's method to genus 1 meshes (which are topologically equivalent to a torus) is well covered by the existing literature, we did not find a similar discussion of the case of meshes with cylindrical topology. Although these can be seen as genus-1 meshes with two boundaries, we find it worthwhile to discuss this case separately, due to its importance for applications in digital geometry reconstruction and because these meshes did not receive much attention in the existing literature.

Motivated by these observations, we present a particularly simple geometric derivation of Tutte's theorem for plane near-triangulations and various extensions thereof, using solely the Euler formula for planar graphs. The starting point of our proof is the combination of the angle excess argument of Richter-Gebert (1996) with edge-collapsing operations (ECOs) to exclude degenerate edges. It is shown that the angle excess argument can deal with degenerate triangles too, once the degenerate edges have been ruled out via ECOs.

In particular, we include the single periodic case – i.e., meshes possessing a cylindrical topology – and we correct a minor inaccuracy in a previous result (Theorem 3.3 of Gortler et al., 2006) concerning Floater-type parameterizations for meshes of genus 1, i.e., doubly periodic surfaces. In fact, the existence and uniqueness of the parameterizations for general (thus potentially non-symmetric) half-edge weights is guaranteed in almost all (26 out of 27) situations, with the exception of genus 1-meshes without boundaries, as we will show in Appendix B.

Fig. 2 summarizes the structure of our proof of Tutte's theorem (shown in green) for plane near-triangulations, which is equivalent to the bijectivity of the associated convex combination mapping (CCM) φ. The gray discs indicate the numbers of the auxiliary propositions and lemmas. Lemma 1, which is the starting point, notes that the vertices can be classified into three types, depending on whether the convex hull of their neighbors' images is a polygon (type (i)), a line segment (type (ii)) or a point (type (iii)).

Only the first case is possible if neither degenerate edges nor degenerate triangles are present. The lemmas and Propositions 2, 3, 4, 8 and 12, which form the backbone of the proof, confirm the bijectivity of φ in this situation. We introduce the angle excess ε_v of a vertex v, which is first shown to be non-negative and then to be zero via Euler's formula. This allows to conclude the local bijectivity of φ, which implies Tutte's theorem in the considered case.

The presence of degenerate triangles is ruled out by Lemma 9 and Proposition 10. Similarly, degenerate edges do not occur: They could be removed by edge collapsing operations (ECOs), whose effect on the CCM is analyzed in Proposition 5. Furthermore, Proposition 11 uses Lemma 7 to show that the resulting clean graph $\check{\mathcal{G}}$ (without type (iii) vertices as noted

[1] His notion of triangulation differs from the one that is used in graph theory, where a triangulation is a planar graph where no edge can be added without losing the planarity property. The Steinitz Theorem guarantees that plane near-triangulations are equivalent to these triangulations.

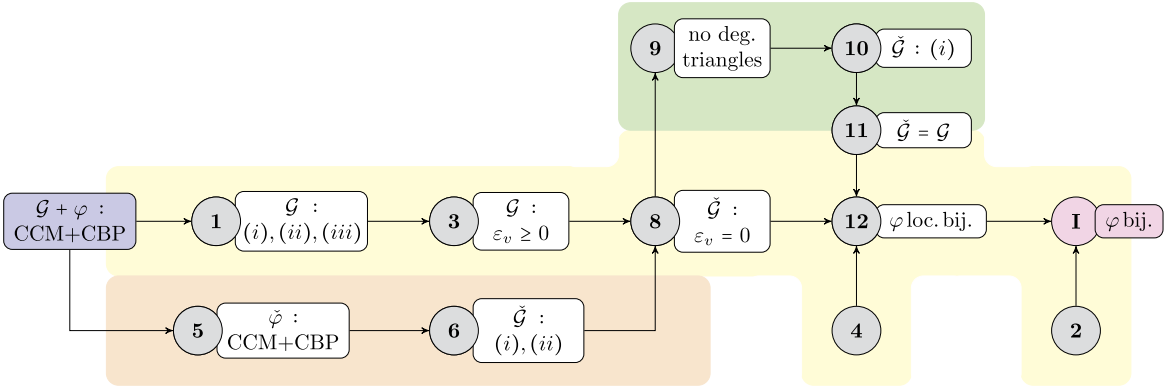

Fig. 2. Structure of the proof of Tutte's theorem (I, magenta) for plane near-triangulations and mappings φ fulfilling the assumptions (left) shown in blue. The yellow (1-4, 8, 11, 12), green (9-11) and orange (5, 6) regions indicate the backbone part and the results needed to rule out degenerate triangles and edges, respectively. (For interpretation of the colors in the figure(s), the reader is referred to the web version of this article.)

in Corollary 6) is identical to the original one. Note that the ECOs are introduced as a proof device only in order to rule out degenerate edges; they are not actually executed in practice.

Sections 2 and 3 of the paper cover these theoretical results. The subsequent sections discuss the different variants of Tutte's Theorem and an application to periodic spline surface fitting.

2. Preliminaries

2.1. Plane near-triangulations

Recall that any embedding of a planar graph with the property that all bounded faces are (possibly curved) triangles is called a *plane near-triangulation* (Hochberg et al., 1995). Throughout this paper, we consider a plane near-triangulation which is 3-connected, and later also generalizations thereof. Note that the embedding is a purely theoretical concept, which is never actually used in practice (e.g., for the application to surface parameterization, which is discussed in Section 6). However, it is needed to establish the underlying theory.

The embedding is represented by a triplet $\mathcal{G} = (V, E, F)$, where $V \subset \mathbb{R}^2$, $E \subset \mathcal{P}(\mathbb{R}^2)$, and $F \subset \mathcal{P}(\mathbb{R}^2)$, are sets of *vertices*, *edges* and *faces*, respectively. Edges and faces are considered as subsets of $\mathbb{R}^2$, i.e., as elements of the power set $\mathcal{P}(\mathbb{R}^2)$.

All the edges are assumed to be smooth curve segments. Besides the exterior face f_{ext}, all the faces are assumed to be *curved triangles* that include their boundaries. The set of faces thus takes the form

$$F = \Delta \cup \{f_{\text{ext}}\},$$

where all the triangles are collected in the set Δ.

For any vertex $v \in V$, we denote with

$$\mathcal{N}_v = \Big(\bigcup \{e \in E : v \in e\} \cap V\Big) \setminus \{v\} \quad \text{and} \quad \Delta_v = \{\delta \in \Delta \mid v \in \delta\}$$

the *set of the neighboring vertices* and the *1-ring neighborhood*, respectively. The union of all the triangles covers the *domain*

$$\Omega = \Big(\bigcup \Delta\Big)^\circ \subset \mathbb{R}^2 .$$

The boundary $\partial\Omega$, which is a simple curved polygon, consists of *boundary edges* E_∂ that connect the *boundary vertices* V_∂. The remaining *inner* vertices V_0 are contained in the interior of the domain. Clearly, V is the disjoint union of V_∂ and V_0.

2.2. Convex combination mappings

We consider a mapping $\varphi : V \to \mathbb{R}^2$ that transforms the vertices $v \in V$ of $\mathcal{G}$ into *points* in $\mathbb{R}^2$. In addition, we consider the piecewise linear continuation

$$x \mapsto \varphi(x) = \sum_{v \in V} h_v(x)\varphi(v), \quad x \in \bar{\Omega},$$

to the full domain, which is obtained by multiplying the vertex images with the associated hat functions $h_v : \bar{\Omega} \to \mathbb{R}$, the construction of which is described in Appendix A. In order to keep the notation simple, we use φ to denote both the mapping of the vertices and its piecewise linear continuation. The construction of the latter ensures that

- these continuous and non-negative functions sum to 1 on $\bar{\Omega}$, taking non-zero-values only within the interior of the 1-ring neighborhood $(\bigcup \Delta_v)^\circ$ of the associated vertex, and
- they assign a unique $|V|$-tuple of values $(h_v(x))_{v \in V}$ to each $x \in \bar{\Omega}$.

Consequently, φ transforms each curved triangle $\delta \in \Delta$ with the vertices u, v and w bijectively into the (possibly degenerate) triangle with vertices $\varphi(u)$, $\varphi(v)$ and $\varphi(w)$ and straight edges.

We recall the definition of a convex combination mapping:

Definition *(Floater, 2003).* The mapping φ is a *convex combination mapping* of $\mathcal{G}$ if the image $\varphi(v)$ of every interior vertex $v \in V_0$ is a convex combination of the images of its neighbors, i.e.,

$$\varphi(v) = \sum_{w \in \mathcal{N}_v} \lambda_{vw}\, \varphi(w) \quad \text{for all } v \in V_0\,, \tag{1}$$

where all weights λ_{vw} are positive and satisfy

$$\sum_{w \in \mathcal{N}_v} \lambda_{vw} = 1\,. \tag{2}$$

The mapping φ has the *convex boundary property* if φ transforms the boundary of Ω homeomorphically into a *strictly convex polygon*.

Note that the weights λ_{vw} are not unique except for vertices of valence three, where they are given by the barycentric coordinates of the vertex with respect to its neighbors. Also, the weights are generally not symmetric, i.e., $\lambda_{vw} \neq \lambda_{wv}$ in general.

2.3. Vertex types

From now on we consider a convex combination mapping φ of $\mathcal{G}$ that satisfies the convex boundary property. The definition from the previous section then implies the following result.

Lemma 1. *For any inner vertex $v \in V_0$ of $\mathcal{G}$, its image $\varphi(v)$ is contained in the relative interior of the convex hull of its neighbors' images $\varphi(\mathcal{N}_v)$. More precisely, it*

(*i*) *is contained in the interior of the convex polygon* $\mathrm{CH}(\varphi(\mathcal{N}_v))$ *if the neighbors' images are not contained in a line,*
(*ii*) *is contained in the interior of the line segment* $\mathrm{CH}(\varphi(\mathcal{N}_v))$ *if the neighbors' images are contained in a line but do not collapse into a single point, or*
(*iii*) *coincides with all its neighbors' images otherwise.*

We will refer to *vertices of type* (*i*), (*ii*) *or* (*iii*), according to the three cases of this lemma.

An edge with end vertices $\acute{v}$ and $\grave{v}$ is said to be *degenerate* (with respect to the mapping φ) if $\varphi(\acute{v}) = \varphi(\grave{v})$. We use the two accents $\acute{}$ and $\grave{}$ to denote the vertices, since edge collapsing operations (see Section 3.2) will be used to merge them. The resulting vertex will be denoted by the descending wedge symbol $\check{}$ that might remind one of the combination of the two accents.

A vertex v is said to be *clean* if all the edges that connect it to the vertices $w \in \mathcal{N}_v$ are non-degenerate. For each vertex $v \in V$, the mapping φ is said to be *locally bijective at* v if its restriction to the 1-ring neighborhood $\bigcup \Delta_v$ is bijective. Clearly, this implies that the vertex v is clean.

3. Tutte's theorem and its proof

We will give a simple proof of Tutte's theorem for the case of plane near-triangulations:

Theorem I *(Tutte, 1963). The mapping φ is bijective if $\mathcal{G}$ is a 3-connected plane near-triangulation and φ is a convex combination mapping that satisfies the convex boundary property.*

In order to prove this result, we will show that φ is locally bijective at all vertices $v \in V$. The theorem then follows from

Lemma 2. *The mapping φ is bijective if and only if it is locally bijective at all vertices $v \in V$.*

Proof. We consider the operator Ψ that transforms functions on $\bar{\Omega}$ into functions on $\varphi(\bar{\Omega})$ via

$$\Psi[f](y) = \sum_{x \in \varphi^{-1}(y)} f(x) \, .$$

The local bijectivity implies that φ transforms any triangle $\delta \in \Delta$ into a regular triangle, thus $\varphi^{-1}(y)$ is finite for any $y \in \varphi(\bar{\Omega})$ and thus Ψ is well-defined. The operator Ψ is linear, since

$$\Psi[\alpha\, f + \beta\, g](y) = \sum_{x \in \varphi^{-1}(y)} \alpha\, f(x) + \beta\, g(x) = \alpha \sum_{x \in \varphi^{-1}(y)} f(x) + \beta \sum_{x \in \varphi^{-1}(y)} g(x) = \alpha\, \Psi[f](y) + \beta\, \Psi[g](y) \, .$$

This implies the identity

$$\Psi[1] = \Psi[\sum_{v \in V} h_v] = \sum_{v \in V} \Psi[h_v] \, ,$$

where we use the fact that the hat functions sum to 1, and the linearity of the operator Ψ.

Note that $\Psi[h_v]$ is the standard (i.e., piecewise linear) hat function on $\varphi(\Delta_v)$, since the mapping φ is locally bijective on all 1-ring neighborhoods, which are the supports of the individual hat functions.

On the one hand, $\Psi[1]$ takes only integer values. On the other hand, the hat functions $\Psi[h_v]$ – and hence also their sum – are continuous. It follows that $\Psi[1]$ is a constant function.

In order to show that $\Psi[1] = 1$, we consider a vertex $p = \varphi(v)$ which is located on the boundary of $\varphi(\bar{\Omega})$. The local bijectivity implies $v \notin V_0$, since otherwise a neighborhood of p would belong to $\varphi(\bar{\Omega})$. The same argument proves that no other point $x \in \Omega$ is mapped into p. Consequently $\Psi[1](p) = 1$ since φ transforms $\partial\Omega$ homeomorphically into a convex polygon.

The proof of the other implication is obvious. □

The remainder of this section presents the proof of local bijectivity, see Proposition 12.

3.1. Local bijectivity at clean vertices

We introduce the notion of the angle excess:

- The *angle excess* of a clean *inner* vertex $v \in V_0$ is defined as

$$\varepsilon_v = \Big(\sum_{\substack{\{u,w\} = \delta \cap N_v \\ \delta \in \Delta_v}} \sphericalangle\, \varphi(u)\, \varphi(v)\, \varphi(w) \Big) - 2\pi \ ,$$

  where $\sphericalangle\, xyz$ denotes the unsigned interior angle. The angle excess measures the difference between the sum of the inner angles at the vertex and the full angle 2π. Note that the angle excess is well defined for clean vertices since no degenerate edges are present.
- Similarly, we define the *angle excess* of a clean *boundary* vertex $v \in V_\partial$ as

$$\varepsilon_v = \Big(\sum_{\substack{\{u,w\} = \delta \cap N_v \\ \delta \in \Delta_v}} \sphericalangle\, \varphi(u)\, \varphi(v)\, \varphi(w) \Big) - \beta_v \ , \tag{3}$$

  where β_v is the inner angle of the boundary polygon $\varphi(\partial\Omega)$ at $\varphi(v)$.

For inner vertices v with a negative angle excess, it is impossible to arrange the neighboring triangles in the plane such that $\varphi(v)$ is located in the relative interior of the convex hull of its neighbors as described in Lemma 1. This observation also applies to boundary vertices, since we consider a strictly convex boundary polygon. This proves the following fact:

Lemma 3. *The angle excesses are always non-negative if φ is a convex combination mapping.*

The classification of the vertices (see Lemma 1) implies the following obvious characterization of local bijectivity:

Proposition 4. *The mapping φ is locally bijective at the vertex $v \in V$ if the angle excess ε_v is zero and all the triangles in $\varphi(\Delta_v)$ are non-degenerate (i.e., they possess non-zero area).*

The absence of degenerate triangles implies that the vertex possesses type (i) and the proof follows from that.

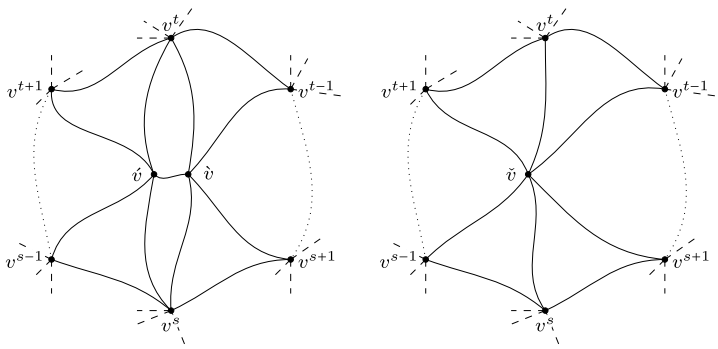

1.) Number the neighboring vertices, $\mathcal{N}_{\acute{v}} \cup \mathcal{N}_{\grave{v}} \setminus \{\acute{v}, \grave{v}\} = \{v^i : i \in \mathbb{Z}/n\}$ counterclockwise around the edge e, where we use indices modulo $n = |\mathcal{N}_{\acute{v}}| + |\mathcal{N}_{\grave{v}}| - 4$. The indices s and t identify the vertices v^s, v^t of the two triangular faces that share the edge e.
2.) Delete the two triangular faces (with vertices $\acute{v}$, $\grave{v}$, v^s and $\acute{v}$, $\grave{v}$, v^t) that share the edge e. Delete all edges that connect $\acute{v}$ or $\grave{v}$ with another vertex.
3.) Create a new vertex $\check{v}$ that replaces $\acute{v}$ and $\grave{v}$ and place it somewhere on the edge e.
4.) Create n new edges connecting $\check{v}$ with v^i, $i \in \mathbb{Z}/n$, and add them to E.
5.) Replace any triangular face in Δ possessing the vertices $\acute{v}$, v^i and v^{i+1} or $\grave{v}$, v^i and v^{i+1} with a face possessing the vertices $\check{v}$, v^i and v^{i+1} and corresponding boundary edges.

Fig. 3. Transformation of a plane near-triangulation by one step of edge collapsing.

3.2. Cleaning the plane near-triangulation $\mathcal{G}$ via edge collapsing

In order to apply the results of the previous section, we will clean the given plane near-triangulation $\mathcal{G}$ by performing *edge collapsing operations* (ECOs) that remove degenerate inner edges and identify the two vertices that are connected by it. Each ECO preserves the numbers of edges and vertices on the domain boundary, and the inner faces remain triangular.

Fig. 3 describes an ECO for an edge e that connects two inner vertices $\acute{v}$ and $\grave{v}$, and this can be extended to the situation where one of these vertices is a boundary vertex. ECOs preserve the planarity and the type of the inner faces, thus they transform the plane near-triangulation into another plane near-triangulation. The property of 3-connectedness, which was assumed for $\mathcal{G}$, may be lost, however.[2] We shall see later that the ECO is a purely theoretical tool needed to prove Theorem I, and not applied in practice.

The ECOs are applied to degenerate edges only, and we will simultaneously modify the mapping φ by assigning the value

$$\varphi(\check{v}) = \varphi(\grave{v}) = \varphi(\acute{v}) \tag{4}$$

to the newly created vertex $\check{v}$ (and unassigning the values of $\grave{v}$ and $\acute{v}$). After applying ECOs to all degenerate edges, we obtain the *clean*[3] plane near-triangulation

$$\check{\mathcal{G}} = (\check{V}, \check{E}, \check{F}) .$$

In analogy to the notation used for the vertices, we will use the descending wedge symbol $\check{}$ to denote the resulting graph, which is obtained after the performing the ECOs. Simultaneously we consider the associated mapping $\check{\varphi}$, which is constructed according to (4), and its piecewise linear continuation, which is again denoted by $\check{\varphi}$.

Proposition 5. *The mapping $\check{\varphi}$ is a convex combination mapping of the clean plane near-triangulation $\check{\mathcal{G}}$, and it also satisfies the convex boundary property.*

Proof. We prove that an ECO of a degenerate edge preserves both the convex combination mapping property and the convex boundary property. This then implies the result since the clean plane near-triangulation is obtained from $\mathcal{G}$ by performing ECOs of this type.

We show that the inner vertices of the modified plane near-triangulation satisfy the convex combination condition (1). First, we analyze the newly created vertex $\check{v}$. It is an inner vertex only if both vertices of the collapsing edge are inner vertices. These vertices then satisfy the equations

$$\varphi(\acute{v}) = \sum_{i=t,\dots,s} \lambda_{\acute{v}v^i}\, \varphi(v^i) + \lambda_{\acute{v}\grave{v}}\, \varphi(\grave{v}) \quad \text{and} \quad \varphi(\grave{v}) = \sum_{i=s,\dots,t} \lambda_{\grave{v}v^i}\, \varphi(v^i) + \lambda_{\grave{v}\acute{v}}\, \varphi(\acute{v}) . \tag{5}$$

Using the fact that the images are identical, $\varphi(\check{v}) = \varphi(\acute{v}) = \varphi(\grave{v})$, we may rearrange them into

$$\varphi(\check{v}) = \varphi(\acute{v}) = \sum_{i=t,\dots,s} \frac{\lambda_{\acute{v}v^i}}{1 - \lambda_{\acute{v}\grave{v}}}\, \varphi(v^i) \quad \text{and} \quad \varphi(\check{v}) = \varphi(\grave{v}) = \sum_{i=s,\dots,t} \frac{\lambda_{\grave{v}v^i}}{1 - \lambda_{\grave{v}\acute{v}}}\, \varphi(v^i) .$$

[2] Such a plane near-triangulation would possess a dividing edge (an inner edge that connects two boundary vertices) or two vertices joined by more than one edge. Some texts use the notion of multigraph to allow multiple edges.

[3] that possesses only clean vertices, hence no degenerate edges.

Finally, we form their average

$$\varphi(\check{v}) = \frac{1}{2}\Big(\sum_{i=t,\dots,s} \frac{\lambda_{\acute{v}v^i}}{1-\lambda_{\acute{v}\grave{v}}}\,\varphi(v^i) + \sum_{i=s,\dots,t} \frac{\lambda_{\grave{v}v^i}}{1-\lambda_{\grave{v}\acute{v}}}\,\varphi(v^i)\Big) = \sum_{i=0,\dots,n-1} \check{\lambda}_{\check{v}v^i}\varphi(v^i)\,,$$

thereby confirming that the new vertex created by assigning $\acute{v}$ to $\check{v}$ satisfies the convex combination condition. Indeed, a short computation confirms that the new weights $\check{\lambda}_{\check{v}v^i}$ sum up to 1 and are positive.

Second, we analyze the remaining two vertices v^s and v^t of the triangles that share the edge $\{\acute{v},\grave{v}\}$. Considering v^t, we modify the convex combination condition which is satisfied prior to the edge collapsing step and obtain

$$v^t = \sum_{v\in\mathcal{N}_{v^t}\setminus\{\acute{v},\grave{v}\}} \lambda_{v^tv}\,v + \lambda_{v^t\acute{v}}\,\acute{v} + \lambda_{v^t\grave{v}}\,\grave{v} = \sum_{v\in\mathcal{N}_{v^t}\setminus\{\acute{v},\grave{v}\}} \lambda_{v^tv}\,v + (\lambda_{v^t\acute{v}} + \lambda_{v^t\grave{v}})\check{v}\,.$$

The same argument applies to v^s. Third, the convex combination conditions of the other inner vertices are still satisfied since their neighbors remain unchanged.

In order to show that the convex boundary property is preserved, it suffices to note that none of the boundary edges is degenerate by definition. Consequently, if an ECO replaces a boundary vertex (by collapsing a degenerate edge that has boundary vertex), then its image point remains unchanged. □

We now use Lemma 1 to obtain the following result, which follows from the absence of degenerate edges:

Corollary 6. *All the inner vertices of the clean plane near-triangulation $\check{\mathcal{G}}$ are of type (i) or (ii).*

Finally we note that the newly created vertices in the clean plane near-triangulation $\check{\mathcal{G}}$, i.e., the ones which are not present in $\mathcal{G}$, are neither vertices of type (i) with zero angle excess nor boundary vertices with zero angle excess:

Lemma 7. *Any vertex of the clean plane near-triangulation $\check{\mathcal{G}}$, which has been created by an ECO, is an inner vertex of type (ii) or possesses positive angle excess.*

Indeed, it is impossible to split (in order to reverse the ECO) an inner vertex of type (i) with zero angle excess into two vertices that satisfy Lemma 1, and a similar argument applies to boundary vertices. We omit the details of the proof.

3.3. Properties of $\check{\mathcal{G}}$

Note that the angle excess is defined for *all* the vertices of $\check{\mathcal{G}}$. The following result is then implied by the Euler formula.

Proposition 8. *All the vertices of $\check{\mathcal{G}}$ have zero angle excess.*

Proof. The clean plane near-triangulation $\check{\mathcal{G}}$ is still 2-connected – since ECOs do not modify the number of boundary edges and vertices – and all its inner faces are (possibly curved) triangles. The Euler formula implies

$$|\check{\Delta}| = 2\,|\check{V}_0| + |\check{V}_\partial| - 2\,.$$

Consequently, the sum of all inner angles of all the image triangles $\check{\varphi}(\delta)$, $\delta\in\check{\Delta}$ (that possess straight edges), fulfills

$$\sum_{v\in\check{V}_0}(2\pi+\varepsilon_v) + \sum_{v\in\check{V}_\partial}(\beta_v+\varepsilon_v) = |\check{\Delta}|\,\pi = (2\,|\check{V}_0| + |\check{V}_\partial| - 2)\,\pi\,.$$

Combining this with the fact that the inner angles β_v, $v\in\check{V}_\partial$, of the boundary $|\check{V}_\partial|$-gon, which possesses the vertices $\check{\varphi}(\check{v})$, $v\in\check{V}_\partial$ and straight edges, sum to $(|\check{V}_\partial|-2)\,\pi$ confirms the identity

$$\sum_{v\in\check{V}}\varepsilon_v = 0\,. \tag{6}$$

Finally we apply Lemma 3 to complete the proof. □

By definition, the clean plane near-triangulation does not possess any degenerate edges (i.e., no edges of zero length). It remains to analyze the existence of degenerate *triangles*, i.e., triangles with zero area. These triangles form the *degenerate sub-graph* of $\check{\mathcal{G}}$. That graph may possess several *edge-connected components*, which can be derived by considering the dual graph, see Fig. 4. We consider one of these components and denote it by $\check{\mathcal{G}}^\star$.

We combine the Euler formula with Corollary 6 to obtain an auxiliary result:

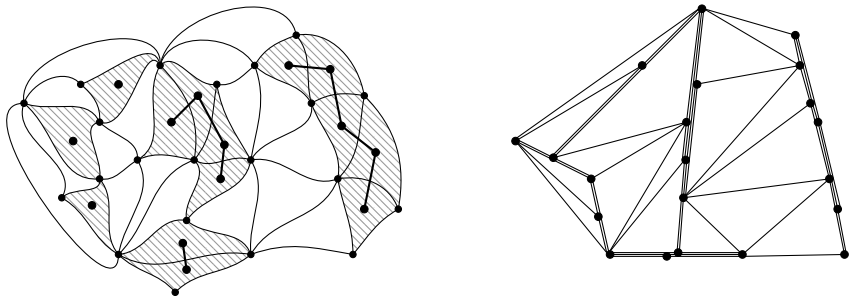

Fig. 4. Left: A plane near-triangulation (left) and its image (right). The degenerate sub-graph (hatched) and the associated dual graph (bold), possessing six (edge-) connected components, are shown. The connected components of the dual graph then correspond to the edge-connected components of the degenerate sub-graph.

Lemma 9. *The boundary of each edge-connected component $\check{\mathcal{G}}^\star$ of the degenerate sub-graph is formed by exactly two edges.*

Proof. The set of faces $\check{F}^\star$ of the sub-graph $\check{\mathcal{G}}^\star = (\check{V}^\star, \check{E}^\star, \check{F}^\star)$ takes the form

$$\check{F}^\star = \check{\Delta}^\star \cup \{f^\star_{\text{ext}}, f^\star_1, \dots, f^\star_{h^\star}\}$$

with triangles $\check{\Delta}^\star \subset \check{\Delta}$ (which are all degenerate, i.e., are transformed into zero area triangles by $\check{\varphi}$), the enlarged exterior face $f^\star_{\text{ext}}$ and a certain number $h^\star$ of interior holes. The boundary of $\check{\mathcal{G}}^\star$ consists of all edges that are incident to exactly one triangle in $\check{\Delta}^\star$. The boundary possesses $b^\star \geq 1$ components. The Euler formula implies the equation

$$|\check{\Delta}^\star| = |\check{E}^\star_\partial| + 2\,|\check{V}^\star_0| + 2b^\star - 4.$$

As in the previous proof, we use this observation to analyze the sum $|\check{\Delta}^\star|\,\pi$ of all inner angles of the triangles' images under $\check{\varphi}$. All the straight angles of the degenerate triangles are attached to the sub-graph's *inner* vertices. Indeed, they cannot occur at boundary vertices (due to the boundary's convexity) or type (i) vertices, and all the triangles in the 1-ring neighborhood of the type (ii) vertices are degenerate. Consequently, we obtain

$$(|\check{E}^\star_\partial| + 2\,|\check{V}^\star_0| + 2b^\star - 4)\,\pi = 2\pi\,|\check{V}^\star_0|\,. \tag{7}$$

This equation can be rewritten as

$$|\check{E}^\star_\partial| + 2b^\star = 4, \tag{8}$$

which implies $b^\star = 1$ and $|\check{E}^\star_\partial| = 2$. □

Now we use the fact that the given plane near-triangulation $\mathcal{G}$ is 3-connected in order to prove that no degenerate triangles exist:

Proposition 10. *All inner vertices of the clean plane near-triangulation $\check{\mathcal{G}}$ are of type (i).*

Proof. Assume that type (ii) vertices exist. The clean plane near-triangulation $\check{\mathcal{G}}$ then possesses the sub-graph $\check{\mathcal{G}}^\star$ that is considered in the previous lemma. The (at most two) boundary vertices of that sub-graph are of type (i). These vertices were not created by an ECO, due to Lemma 7 and Proposition 8, thus they are already present in the original plane near-triangulation $\mathcal{G}$. Removing these vertices, however, would split the plane near-triangulation $\mathcal{G}$ into two connected components, in contradiction to the assumption that it is 3-connected. □

3.4. Local bijectivity of $\mathcal{G}$

Finally we transfer the properties of the clean plane near-triangulation $\check{\mathcal{G}}$ to the original one, by noting that they are in fact the same:

Proposition 11. *The given plane near-triangulation $\mathcal{G}$ does not possess any degenerate edge, hence the clean plane near-triangulation $\check{\mathcal{G}}$ is equal to the original one.*

Proof. According to the previous proposition combined with Lemma 7, none of the inner vertices of the clean plane near-triangulation was created by an ECO. That lemma also ensures that no boundary vertex was created by an ECO since all the angle excesses are zero by Proposition 8. □

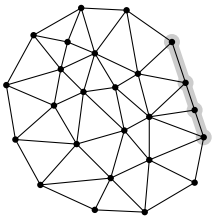

Fig. 5. Convex, but not strictly convex.

This result allows us to complete the proof of local bijectivity, thus of Theorem I:

Proposition 12. *The mapping φ is locally bijective at all vertices of $\mathcal{G}$.*

Proof. All results about the clean plane near-triangulation $\check{\mathcal{G}}$ apply to the given plane near-triangulation $\mathcal{G}$ and its associated convex combination mapping φ, due to previous lemma. In particular, all the vertices are clean by definition of $\mathcal{G}$, and have zero angle excess according to Proposition 8. No degenerate triangles are present, because all the inner vertices are of type (i) by Proposition 10. Consequently, φ is locally bijective at all vertices, since it satisfies the conditions of Proposition 4. □

4. The 27 variants of Theorem I

We discuss several variants, most of which are already covered by the literature:

Theorem II. *The mapping φ is bijective if one or more of the Assumptions A–F are satisfied.*

The first three assumptions are related to the properties of the mapping φ. The remaining assumptions will relax the properties of the plane near-triangulation as well.

Theorem I remains valid if adjacent collinear edges of the boundary polygon $\varphi(\partial\Omega)$ are present, see Fig. 5:

Assumption A *(Floater, 2003).* The boundary polygon $\varphi(\partial\Omega)$ is convex, but not necessarily strictly convex.

Proof. The strict convexity was used only in two places. First, it was needed for proving Lemma 3. It is easy to see that the proof remains intact when relaxing the assumption to a convex boundary. Second, we used it in the proof of Lemma 9. We split the set of boundary vertices into two subsets $\check{V}^\star_\partial = \check{V}^\star_{\partial,\pi} \cup \check{V}^\star_{\partial,0}$ consisting of the vertices that contribute the angle π or 0 to the adjacent (degenerate) triangles in $\check{\Delta}^\star$. Under Assumption A, the second subset $\check{V}^\star_{\partial,\pi}$ may be non-empty. Consequently, equation (7) has to be rewritten as

$$(|\check{E}^\star_\partial| + 2\,|\check{V}^\star_0| + 2b^\star - 4)\,\pi = 2\pi\,|\check{V}^\star_0| + \pi\,|\check{V}^\star_{\partial,\pi}|\,,$$

which implies

$$|\check{E}^\star_\partial| + 2b^\star = 4 + |\check{V}^\star_{\partial,\pi}|\,.$$

The original proof remains valid if $|\check{V}^\star_{\partial,\pi}| = 0$. Otherwise, we split the set $\check{E}^\star_\partial$ into boundary edges on the domain boundary $\check{E}^\star_{\partial,\partial}$ and the remaining boundary edges $\check{E}^\star_{\partial,0}$ and obtain

$$|\check{E}^\star_{\partial,0}| + \underbrace{|\check{E}^\star_{\partial,\partial}| - |\check{V}^\star_{\partial,\pi}|}_{\geq 1} + 2b^\star = 4\,. \tag{9}$$

Therefore $|\check{E}^\star_{\partial,0}| = 1$ and $b^\star = 1$, since at least $|\check{V}^\star_{\partial,\pi}| + 1$ boundary edges on the domain boundary must be present. Removing the edge $\check{E}^\star_{\partial,0}$ and its vertices, which are both located on the domain boundary, would split the plane near-triangulation $\mathcal{G}$ into two connected components, in contradiction to the assumption that it is 3-connected. □

The second generalization relaxes the assumption that the given plane near-triangulation is 3-connected. We say that the plane near-triangulation $\mathcal{G}$ is *weakly 3-connected* if it is 2-connected and any pair of vertices whose removal causes $\mathcal{G}$ to split into several components is connected by a *dividing edge*, i.e., by an inner edge joining two boundary vertices, see Fig. 6.

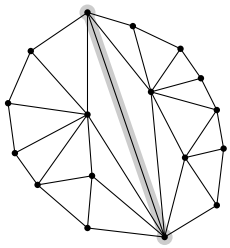

Fig. 6. Dividing edge.

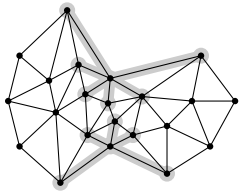

Fig. 7. Reflex vertex lies in the convex hull of its neighbors.

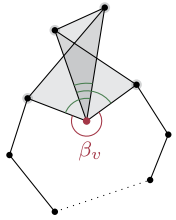

Fig. 8. Reflex vertex (purple) and its neighbors (green) with zero angle excess (purple angle equals sum of green angles). Zero angle excess does not imply local bijectivity in this case.

Assumption B *(Floater, 2003).* The plane near-triangulation $\mathcal{G}$ may be weakly 3-connected, provided that the boundary polygon $\varphi(\partial\Omega)$ does not contain any of the dividing edges' images.

Proof. The fact that $\mathcal{G}$ is 3-connected was used to prove the degenerate sub-graph is empty, by showing that no edge-connected component $\check{G}^\star$ of this graph exists. In order to show that Assumption B is also sufficient, we assume that the degenerate sub-graph has at least one edge-connected component $\check{G}^\star$.

On the one hand, for a sub-graph $\check{G}^\star$ without edges on the domain boundary, the proofs of Lemma 9 and Proposition 10 remain intact. On the other hand, for a sub-graph $\check{G}^\star$ with edges on the domain boundary, we need to re-visit the previous proof. There we already noted that $|\check{E}^\star_{\partial,0}| = 1$. Consequently, the boundary of $\check{G}^\star$ consists of single dividing edge, combined with edges $\check{E}^\star_{\partial,\partial}$ on the domain boundary. However, the image of $\check{G}^\star$ collapses into a line segment since all triangles $\check{\Delta}^\star$ are degenerate, thereby contradicting the assumption that the boundary polygon $\varphi(\partial\Omega)$ does not contain the dividing edge's image. □

We say that the boundary polygon $\varphi(\partial\Omega)$ possesses a *reflex vertex* if the inner angle at that point exceeds π, see Fig. 7

Assumption C *(Gortler et al., 2006).* The boundary polygon $\varphi(\partial\Omega)$ may possess one or more reflex vertices, provided that these are contained in the interior of the convex hull of their neighbors.

Proof. First, the convexity of the boundary was needed to prove the non-negativity of the angle excess at boundary vertices in Lemma 3. Since this proof no longer applies to reflex vertices, the additional condition that these are contained in the interior of the convex hull of their neighbors is needed.

Second, we used the convexity of the boundary to conclude that a zero angle excess implies local bijectivity at boundary vertices. This is generally not true for reflex vertices, see Fig. 8. The additional condition resolves this situation.

Third, the presence of reflex boundary vertices leads to another case in the proof of Lemma 7. Again, it is easy to show that these vertices are not created by ECOs.

Furthermore, under Assumption A, the additional condition ensures that none of the reflex vertices is contained in $\check{V}^{\star}_{\partial,\pi}$, see Fig. 7 and Fig. 5. Hence, the component of the degenerate sub-graph has $|\check{V}^{\star}_{\partial,\pi}|+1$ edges on the domain boundary if $|\check{V}^{\star}_{\partial,\pi}| \neq 0$ as noted when discussing Assumption A. □

If reflex vertices are allowed, one may consider domain boundaries that have several connected components. Thus, besides the un-bounded exterior face, there can be one or more bounded exterior faces. This leads to *generalized* plane near-triangulations.

Assumption D *(Gortler et al., 2006).* The boundary $\partial\Omega$ may consist of several connected components and φ transforms them homeomorphically into simple polygons, which are mutually disjoint.

Proof. The proof of Proposition 8 has to be adapted as follows. On the one hand the number of triangles of a connected planar domain with h holes satisfies

$$|\check{\Delta}| = 2\,|\check{V}_0| + |\check{V}_\partial| + 2h - 2\,.$$

On the other hand, the inner angles of the boundary polygon and the exterior angles of the h polygons representing the holes sum to $(|\check{V}_\partial|+2h-2)\,\pi$. Again, we combine these two observations to prove the identity (6) with the help of Lemma 3 and Assumption C. □

In order to combine this assumption with Assumption B, need to reformulate it as follows:

Assumption B′. The generalized plane near-triangulation $\mathcal{G}$ may be weakly 3-connected, provided that none of the boundary polygons in $\varphi(\partial\Omega)$ contains any of the dividing edges' images.

Note that this is automatically satisfied if a dividing edge connects two vertices on *different* connected components of the boundary.

Finally we discuss a generalization to special classes of infinite generalized plane near-triangulations. First, we note that Lemma 2 applies to infinite generalized plane near-triangulations also.

Lemma 2′. *Local bijectivity implies global bijectivity also if the generalized plane near-triangulation $\mathcal{G}$ is infinite.*

Proof. Assume that φ transforms two points $x, x' \in \bar{\Omega}$ into a single image point $\varphi(x) = \varphi(x')$. This is a contradiction to Lemma 2, since these two points are then contained in a (finite) PNT. □

The special classes we consider are characterized by periodicity properties. We distinguish between periodicity with respect to one or two directions, as follows:

The generalized plane near-triangulation $\mathcal{G}$ is said to be *t-periodic* if $\mathcal{G} + t\,\mathbb{Z} = \mathcal{G}$, where $t \in \mathbb{R}^2 \setminus \{(0,0)\}$ is some vector. However, we consider only generalized plane near-triangulations which are still finite in the sense that all the vertices, edges and triangular faces can be obtained as translates of a finite number of vertices, edges and triangular faces, respectively. Note that the numbers of vertices, edges and faces of such graphs refer to the number of equivalence classes with respect to the considered translations.

Additionally, the mapping φ is said to be *t-quasi-periodic*, if

$$\varphi(v + t) = \varphi(v) + t_\varphi$$

holds for all vertices $v \in V$, where $t_\varphi \in \mathbb{R}^2 \setminus \{(0,0)\}$ is some vector.

A domain defined by a t-periodic generalized plane near-triangulation $\mathcal{G}$ possesses *two* unbounded external faces with associated boundary components, since we only consider generalized plane near-triangulations that are connected. Clearly, this is not possible if the boundary is assumed to be strictly convex. In the simplest case the boundary is mapped to two parallel straight lines and this is covered by Assumption A. Configurations with more general boundaries, and possibly even with additional interior boundary components, are covered by Assumptions C and Assumption D.

Assumption E. The generalized plane near-triangulation $\mathcal{G}$ is t-periodic, the mapping φ is t-quasi-periodic and the images of the external faces' boundaries are disjoint.

Proof. First we adapt the proof of Proposition 8. The number of triangles in the t-periodic case satisfies

$$|\check{\Delta}| = 2\,|\check{V}_0| + |\check{V}_\partial|\,,$$

while the inner angles β_v with $v \in V_\partial$ of the two boundary polygons (which are both t-periodic) sum to $|\check{V}_\partial|\,\pi$. Again, we may combine these two facts to confirm the identity (6).

Second, we revisit the version of the proof of Lemma 9 that was modified in view of Assumption A. The sub-graph $\check{\mathcal{G}}^\star$ is either bounded or unbounded. In the bounded case, the degenerate sub-graph contains all its t-translates. Nevertheless, it suffices to analyze one component only, and this can be done exactly as in the original proof. In the unbounded case we arrive again at equation (9) but with $b \geq 2$. Solutions are only available if $|\check{E}^\star_{\partial,\partial}| = |\check{V}^\star_{\partial,\pi}|$, which is the case if the degenerate sub-graph shares an entire boundary with the domain boundary. Even in this case, however, we get $|\check{E}^\star_{\partial,0}| = 0$. Hence, the only possibility is a degenerate sub-graph that shares *both* boundaries with $\check{\mathcal{G}}$, but this is excluded by the assumption. □

The generalized plane near-triangulation $\mathcal{G}$ is said to be *doubly* (s,t)*-periodic* if $\mathcal{G} + s\,\mathbb{Z} + t\,\mathbb{Z} = \mathcal{G}$, where $s, t \in \mathbb{R}^2$ are two linearly independent vectors. As before, we consider only generalized plane near-triangulations which are finite in the sense that all the vertices, edges and triangular faces can be obtained as translates of a finite number of vertices, edges and triangular faces, respectively. Again, the numbers of vertices, edges and faces refer to the number of equivalence classes with respect to the considered translations.

Additionally, the mapping φ is said to be *doubly* (s,t)*-quasi-periodic*, if

$$\varphi(v+s) = \varphi(v) + s_\varphi \quad \text{and} \quad \varphi(v+t) = \varphi(v) + t_\varphi$$

holds for all vertices $v \in V$ and two vectors $s_\varphi, t_\varphi \in \mathbb{R}^2$, which are linearly independent.

It follows that the domain does not possess an unbounded external face. First we consider generalized plane near-triangulations without boundaries.

Assumption F *(Gortler et al., 2006).* The generalized plane near-triangulation $\mathcal{G}$ is doubly (s,t)-periodic and the mapping φ is doubly (s,t)-quasi-periodic.

Proof. Again, we adapt the proof of Proposition 8. The Euler formula for doubly periodic generalized plane near-triangulations can be used to show that

$$|\check{\Delta}| = 2\,|\check{V}|\,,$$

since every vertex is an inner vertex. Hence, the sum of all inner angles of all triangles fulfills

$$\sum_{v \in \check{V}} (2\pi + \varepsilon_v) = |\check{\Delta}|\,\pi = 2\,|\check{V}|\,\pi\,,$$

and Eq. (6) follows again, which implies zero angle excesses according to Lemma 3.

Second, we revisit the version of the proof of Lemma 9. The sub-graph $\check{\mathcal{G}}^\star$ is either bounded or unbounded. In the bounded case, the degenerate sub-graph contains all its (s,t)-translates. Nevertheless, it suffices to analyze one component only, and this can be done exactly as in the original proof. In the unbounded case there are two possibilities. The symmetry group of the considered sub-graph is generated by either one or two translations. In the first situation, we arrive again at equation (8) but with $b^\star \geq 2$, since at least two boundary components would be present. This leads to a contradiction, as $|E^\star_\partial|$ has to be positive. In the other situation, the Euler formula implies the equation

$$|\check{\Delta}^\star| = |\check{E}^\star_\partial| + 2\,|\check{V}^\star_0| + 2b^\star\,.$$

Once more, we use this observation to analyze the sum $|\check{\Delta}^\star|\,\pi$ of all inner angles. All the straight angles of the degenerate triangles are attached to the sub-graph's *inner* vertices. Consequently, we obtain

$$(|\check{E}^\star_\partial| + 2\,|\check{V}^\star_0| + 2b^\star)\,\pi = 2\pi\,|\check{V}^\star_0|\,.$$

This equation can be rewritten as

$$|\check{E}^\star_\partial| + 2b^\star = 0,$$

which leads to a contradiction. □

Finally, we analyze the possibilities to combine the Assumptions A–F:

- First we consider combinations without Assumptions E or F, i.e., the non-periodic case. Only the 12 combinations shown in Fig. 9 are possible, since Assumption D implies Assumption C.
- Second, we analyze combinations with Assumption E, i.e., the periodic case. Here we get a similar picture as in the previous case, except for the missing cases with no assumption and with only Assumption B. Indeed, the periodic case is only possible if at least one of the Assumptions A and C is satisfied.

	A	B	C	D	E	F
1						
2	✓					
3		✓				
4			✓			
5	✓	✓				
6	✓		✓			
7	✓	✓	✓			
8	✓		✓	✓		
9		✓	✓			
10		✓	✓	✓		
11			✓	✓		
12	✓	✓	✓	✓		
13	✓				✓	
14			✓		✓	
15	✓		✓		✓	
16	✓	✓			✓	
17		✓	✓		✓	
18			✓	✓	✓	
19	✓	✓	✓		✓	
20		✓	✓	✓	✓	
21	✓		✓	✓	✓	
22	✓	✓	✓	✓	✓	
23						✓
24			✓	✓		✓
25	✓		✓	✓		✓
26		✓	✓	✓		✓
27	✓	✓	✓	✓		✓

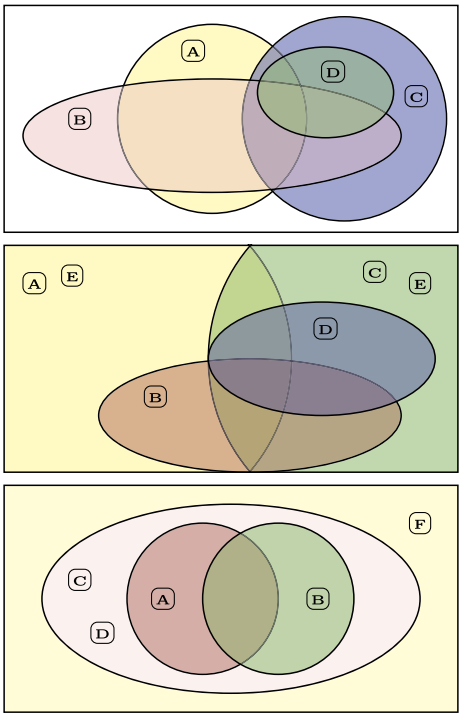

Fig. 9. Left: The 27 possible combinations of Assumptions A to F. Right: Relation between the possibilities without E and F (top), with E (center), and with F (bottom).

- Third, we consider combinations with Assumption F, i.e., the doubly periodic case, where Assumptions C and D can only be used simultaneously and are moreover implied by A and B. This leaves only five possibilities.

Summing up, *we arrive at* 27 *variants of Tutte's theorem for plane near-triangulations.*

5. Existence and uniqueness

So far bijectivity of convex combination mappings was studied. This section focuses on the existence and computation of convex combination mappings from given data, both in the periodic and in the non-periodic case.

5.1. Non-periodic case

Consider a given 3-connected generalized plane near-triangulation $\mathcal{G}$ with associated weights λ_{vw} that satisfy (2). Furthermore, the images $b_v = \varphi(v)$ of the boundary vertices $v \in V_\partial$ are also given.

Theorem III. *There exists a unique convex combination mapping of $\mathcal{G}$ that respects the given weights and boundary data.*

Proof. The convex combination mapping is determined by the vertices' images $p_v = \varphi(v)$ for all $v \in V$. These images satisfy the linear equations

$$\begin{cases} p_v = b_v & \text{if} \quad v \in V_\partial \\ p_v - \displaystyle\sum_{w \in \mathcal{N}_v} \lambda_{vw} p_w = 0 & \text{if} \quad v \in V_0 \,. \end{cases}$$

We obtain two linear systems, one for each of the two coordinates, sharing the same coefficient matrix. This matrix is a weakly chained diagonally dominant (WCDD) square matrix, hence regular (Shivakumar and Chew, 1974; Taussky, 1949). □

5.2. The t-periodic case

This case is characterized by Assumption E. Again, we consider a given generalized plane near-triangulation $\mathcal{G}$ with associated weights and images of the boundary vertices. Additionally, we assume that these data are compatible with the t-periodicity, i.e., they satisfy $\lambda_{vw} = \lambda_{(v+t)(w+t)}$ and $b_{v+t} = b_v + t_\varphi$, where t_φ is also given.

Theorem IV. *There exists a unique convex combination mapping of the t-periodic generalized plane near-triangulation $\mathcal{G}$ that respects the given weights and boundary data.*

Proof. The t-periodicity induces an equivalence relation on the set of vertices. It suffices to consider one representative of each vertex. More precisely, we select a set $\tilde{V} \subset V$, which is chosen as small as possible, such that $\tilde{V} + t\,\mathbb{Z} = V$. Consequently, for every vertex $v \in V$ there exists a unique integer z_v such that $v + t\,z_v \in \tilde{V}$.

The convex combination mapping is determined by the vertices' images $p_v = \varphi(v)$ for all $v \in \tilde{V}$. These images satisfy the linear equations

$$\begin{cases} p_v = b_v & \text{if} \quad v \in V_\partial \cap \tilde{V} \\ p_v - \sum\limits_{w \in \mathcal{N}_v} \lambda_{vw}\, p_{w+t\,z_w} = -t_\varphi \sum\limits_{w \in \mathcal{N}_v} \lambda_{vw}\, z_w & \text{if} \quad v \in V_0 \cap \tilde{V} \end{cases} \tag{10}$$

Again, we obtain two linear systems, one for each of the two coordinates, sharing the same coefficient matrix. This matrix is a weakly chained diagonally dominant (WCDD) square matrix, thus regular. □

5.3. The doubly (s,t)-periodic case

This case is characterized by Assumption F. Once more, we consider a given generalized plane near-triangulation $\mathcal{G}$ with associated weights and images of the boundary vertices. Additionally, we assume that these data are compatible with the (s,t)-periodicity, i.e., they satisfy $\lambda_{vw} = \lambda_{(v+s)(w+s)} = \lambda_{(v+t)(w+t)}$ and $b_{v+s} = b_v + s_\varphi$ and $b_{v+t} = b_v + t_\varphi$ where s_φ and t_φ are also given.

Theorem V. *There exists a unique convex combination mapping of the (s,t)-periodic generalized plane near-triangulation $\mathcal{G}$ that respects the given weights and boundary data if $V_\partial \neq \emptyset$.*

Proof. The (s,t)-periodicity induces an equivalence relation $\sim$ on the set of vertices. Again it suffices to consider one representative of each vertex. Thus, we select a set $\tilde{V} \subset V$, which is chosen as small as possible, such that $\tilde{V} + s\,\mathbb{Z} + t\,\mathbb{Z} = V$. Consequently, for every vertex $v \in V$ there exist unique integers y_v and z_v such that $v + s\,y_v + t\,z_v \in \tilde{V}$.

The convex combination mapping is determined by the vertices' images $p_v = \varphi(v)$ for all $v \in \tilde{V}$. These images satisfy the linear equations

$$\begin{cases} p_v = b_v & \text{for all} \quad v \in V_\partial \cap \tilde{V} \\ p_v - \sum\limits_{w \in \mathcal{N}_v} \lambda_{vw}\, p_{w+s\,y_w+t\,z_w} = -s_\varphi \sum\limits_{w \in \mathcal{N}_v} \lambda_{vw}\, y_w - t_\varphi \sum\limits_{w \in \mathcal{N}_v} \lambda_{vw}\, z_w & \text{for all} \quad v \in V_0 \cap \tilde{V} \end{cases} \tag{11}$$

Once more, we obtain two linear systems, one for each of the two coordinates, sharing the same coefficient matrix. This matrix is a weakly chained diagonally dominant (WCDD) square matrix, therefore regular. □

Note that this proposition does not apply to the case $V_\partial = \emptyset$ that corresponds to Assumption F without any further assumption (i.e., without Assumptions C and D, see Fig. 9, right). This particular case is addressed in Appendix B.

6. Periodic parameterization and surface fitting

We demonstrate the practical relevance of the t-periodic case for periodic parameterization and surface approximation of scanned aircraft engine parts. We assume that the measurement points of the optical scanning machine have been processed in such a way that the region of interest is given in the form of a triangular mesh of cylindrical topology: it has exactly two holes, each of them bounded by a closed loop. We assume that the two boundary loops inherit their orientation from the half-edges. The task is to approximate this surface mesh with a periodic spline surface, in order to prepare further processing.

First, we need to parameterize the vertices $v \in V$ of the mesh by assigning a point $p_v \in [0,1]^2$ in parameter space to each of them. Second, we invoke a standard surface fitting algorithm such as least-square approximation.

Note that the starting point of the procedure is a triangular mesh in three-dimensional space possessing a cylindrical topology, and not a t-periodic generalized plane near-triangulation. However, it is clear that these two objects are equivalent, and we will simply adapt the terminology of Section 5.2 accordingly. In particular, we will use V, E and Δ to denote the sets of vertices, edges and triangles, respectively.

The parameterization step starts by assigning points in parameter space to the boundary vertices. One chooses a reference point on each of the boundary loops (possibly on an edge) and assigns the points $(0,0)^T$ or $(0,1)^T$ to it, respectively. The vertices of the two boundary loops are then assigned to points on the lower and upper edge of the unit square using a relative chord length parameterization.[4] Note that one needs to reverse the orientation of one of the two boundary loops.

We generate a strip of triangles, which connects the two edges that contain the reference points on the boundary loops. These two edges serve as the southern and northern boundary of the strip, respectively, while the two polygons connecting their endpoints form the eastern and western boundary, respectively. The inner edges of the strip are called *strip edges*. Note that a strip edge always connects vertices on the eastern and western boundary.

We compute the points in the parameter space assigned to the inner vertices by solving the system of equations

$$\begin{cases} p_v = b_v & \text{if} \quad v \in V_\partial \\ p_v - \sum_{w \in \mathcal{N}_v} \lambda_{vw} p_w = (1,0)^T \sum_{w \in \mathcal{N}_v} \lambda_{vw} z_{vw} & \text{if} \quad v \in V_0 \end{cases}$$

where

$$z_{vw} = \begin{cases} -1 & \text{if } v \text{ and } w \text{ are connected by a strip edge from east to west,} \\ +1 & \text{if } v \text{ and } w \text{ are connected by a strip edge from west to east,} \\ 0 & \text{otherwise.} \end{cases}$$

Similarly to the results of Tong et al. (2006) one can show that the result is independent of the choice of the strip.

For the tensor-product spline surface fitting we use the standard least-square approximation regularized by the thin plate energy (Hoschek and Lasser, 1993). As an example, we have taken a triangular mesh with 19,304 vertices obtained from a 3D scan of an aircraft engine turbine blade with a length of approx. 10 cm. In the first case, we have manually designed a curve that represents the periodic interface and parameterized the mesh with this curve imprinted by using the CGAL library (Saboret et al., 2019). In the second case, we used the method we have just described. In both cases, the boundaries are parameterized by scaled chord length and the weights λ_{vw} are selected using Floater's shape-preserving parameterization method (Floater, 1997). We used the G+Smo library (Jüttler et al., 2014) for surface fitting with periodic bi-cubic splines on a tensor-product grid consisting of uniform (which are clamped in vertical direction) knot vectors with 100×25 simple interior knots, respectively, and we set the regularization weight $\lambda = 10^{-8}$.

While the resulting surfaces were quite similar, Fig. 10 (top row) shows the difference in the parameterizations near the interface. For the left surface, the use of a $\mathcal{C}^2$-smooth function to approximate the data leads to oscillations, as can be seen in the reflection lines in Fig. 10 (bottom row). For this surface, 79% of the points were within the tolerance of 10 µm, compared to 81% in the case of the periodic parameterization (right surface). The maximum distances evaluate to 138 µm and 137 µm, respectively.

The difference between the methods is yet more pronounced in the synthetic example shown in Fig. 1. The hyperboloid has the height of 0.75 m and radius 0.25 and its triangulation with 924 vertices is shown in Fig. 1 left. The fitting with 31×31 interior knots and $\lambda = 10^{-8}$ on a non-periodic parameterization lead to 77% of points within the tolerance of 10 µm and the maximum error of 0.21 mm, see Fig. 1, second and third from left. The same fitting on a periodic parameterization lead to 100% points within the tolerance and maximum error 0.1 µm, see Fig. 1, fourth and fifth from left.

7. Conclusion

Motivated by the applications of Floater's method to periodic spline surfaces, we presented a particularly simple geometric derivation of Tutte's theorem for plane near-triangulations and various extensions thereof, using solely the Euler formula for planar graphs. After using edge-collapsing operations to exclude degenerate edges, we combined the Euler formula with an angle excess argument to prove local bijectivity. Future work will be devoted to surfaces of higher genus and meshes with more general faces than triangles, and we will explore applications in spline surface fitting.

CRediT authorship contribution statement

All authors: Conceptualization, Methodology, Visualization, Software, Writing.

Declaration of competing interest

The authors declare that they have no known competing financial interests or personal relationships that could have appeared to influence the work reported in this paper.

[4] Other standard schemes (e.g., uniform or centripetal parameterization) may be used as well.

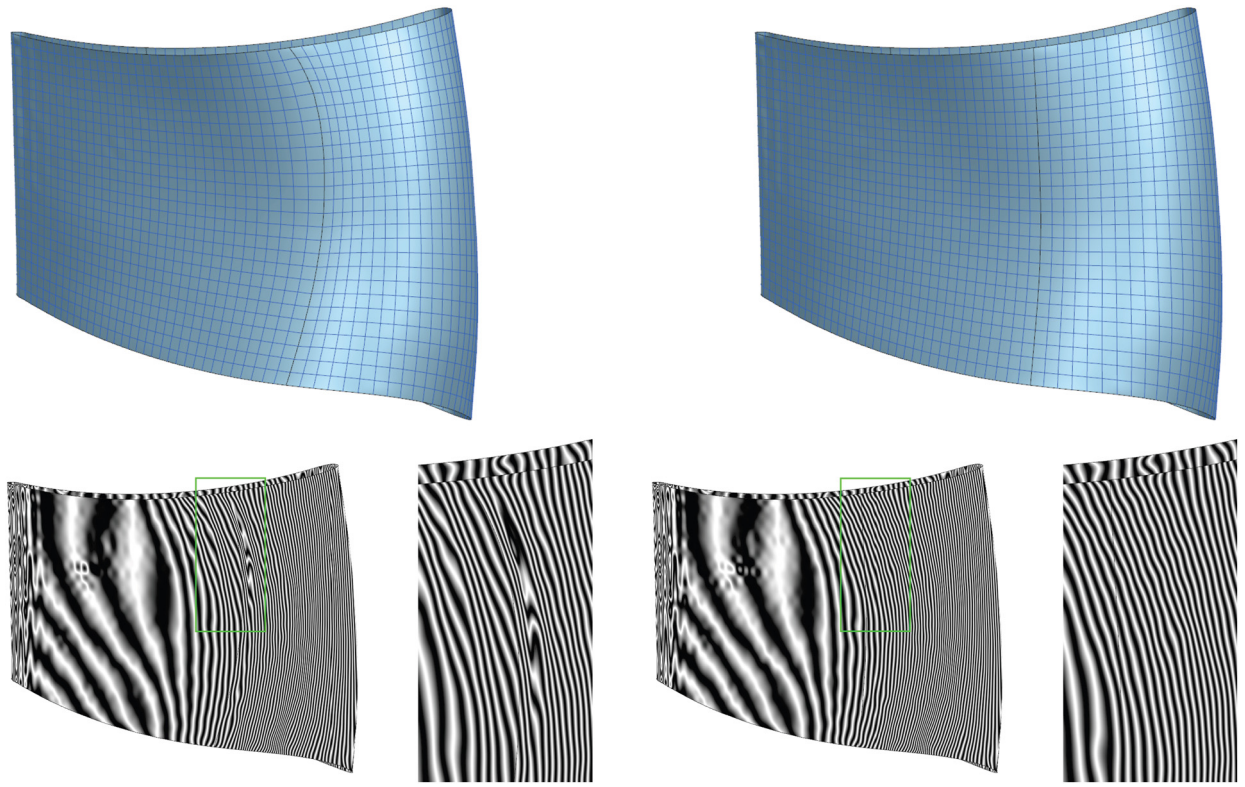

Fig. 10. Top row: periodic fitting of a standard (left) and of a periodic (right) parameterization. Bottom row: Reflection lines of the approximation surface and a closer view of the indicated area, using the standard (left) and the periodic (right) parameterization.

Acknowledgement

Supported by the Austrian Science Fund (FWF) through NFN S117 "Geometry + Simulation".

Appendix A. Hat functions on curved triangulations

For each curved triangle $\delta^{ijk} \in \Delta$ with vertices $v^i, v^j, v^k \in V$, we define the associated diffeomorphism as a harmonic mapping $D^{ijk} : \delta^{ijk} \to T$, where T is some master triangle with certain vertices $w^1, w^2, w^3 \in \mathbb{R}^2$, see Fig. A.11. The diffeomorphism is described by the barycentric coordinates

$$D^{ijk}(x) = \beta^1(x)\, w^1 + \beta^2(x)\, w^2 + \beta^3(x)\, w^3\,, \qquad \beta^1(x) + \beta^2(x) + \beta^3(x) = 1\,,$$

of the image of a point $x \in \delta^{ijk}$ with respect to T. The three functions β^i are simply the *harmonic barycentric coordinates* with respect to the curved triangle, see DeRose and Meyer (2006). These are harmonic functions that satisfy the boundary conditions

$$\begin{aligned}
&\beta^1(x) = \mathcal{L}(e^{ij}_{jx})/\mathcal{L}(e^{ij}), \quad \beta^2(x) = \mathcal{L}(e^{ij}_{ix})/\mathcal{L}(e^{ij}), \quad \text{and} \quad \beta^3(x) = 0 \text{ on the edge } e^{ij}\,,\\
&\beta^2(x) = \mathcal{L}(e^{jk}_{kx})/\mathcal{L}(e^{jk}), \quad \beta^3(x) = \mathcal{L}(e^{jk}_{jx})/\mathcal{L}(e^{jk}), \quad \text{and} \quad \beta^1(x) = 0 \text{ on the edge } e^{jk}\,,\\
&\beta^3(x) = \mathcal{L}(e^{ki}_{ix})/\mathcal{L}(e^{ki}), \quad \beta^1(x) = \mathcal{L}(e^{ki}_{kx})/\mathcal{L}(e^{ki}), \quad \text{and} \quad \beta^2(x) = 0 \text{ on the edge } e^{ki}\,.
\end{aligned} \tag{A.1}$$

In this equation, x is any point on an edge $e^{m,n}$ that connects any two vertices v^m, v^n of the curved triangle δ^{ijk}. The point x splits the edge $e^{m,n}$ into two segments $e^{m,n}_{m,x}$ and $e^{m,n}_{n,x}$, and $\mathcal{L}(.)$ denotes the length of a curve segment, see Fig. A.11.

We define the hat function of a vertex v as

$$h_v(x) = \begin{cases} \beta^r(x) & \text{if } x \in \delta^{ijk} \text{ and } D^{ijk}(v) = w^r \\ 0 & \text{otherwise} \end{cases} \tag{A.2}$$

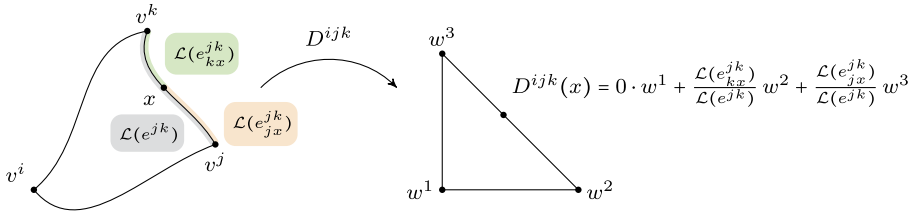

Fig. A.11. Master triangle and barycentric coordinates.

The condition (A.1) is needed to guarantee that h_v is well defined also on the inner edges of the 1-ring neighborhood of v. One gets the same value independent of which of the curved triangles that share this edge is considered in (A.2).

Appendix B. Existence of a convex combination mapping in the doubly periodic case without boundaries

We show that the results concerning existence and uniqueness of convex combination mappings do not extend to this case for general weights, in contrary to what is claimed in Gortler et al. (2006). Existence of convex combination mappings requires special classes of weights, such as quasi-symmetric ones.

We rewrite the linear equations (11) in order to investigate the existence of solutions if no boundaries are present, i.e., if $V_\partial = \emptyset$. The periodicity defines an equivalence relation

$$x \sim x' \quad \text{iff} \quad x - x' \in s\mathbb{Z} + t\mathbb{Z} \,.$$

We identify vertices, edges and triangular faces of G that are equivalent according to $\sim$ and obtain classes $\tilde{v} \in \tilde{V}$, $\tilde{e} \in \tilde{E}$, $\tilde{\delta} \in \tilde{\Delta}$ of equivalent vertices, edges, and triangular faces. For each edge $e \in \tilde{E}$, we introduce the two differences

$$d_{\tilde{v}\tilde{w}} = \varphi(w) - \varphi(v) \quad \text{and} \quad d_{\tilde{w}\tilde{v}} = \varphi(v) - \varphi(w) \,,$$

where the vertices $\tilde{v}, \tilde{w} \in \tilde{V}$ are the endpoints of that edge $\tilde{e} \in \tilde{E}$, and the vertices $v, w \in V$ are the endpoints of a representative $e \in \tilde{e}$ thereof. The two differences per edge satisfy

$$d_{\tilde{v}\tilde{w}} + d_{\tilde{w}\tilde{v}} = 0 \,. \tag{B.1}$$

For each triangle $\tilde{\delta} \in \tilde{\Delta}$ with vertices $\tilde{u}\tilde{v}\tilde{w}$, which are ordered counterclockwise, we get the equation

$$d_{\tilde{u}\tilde{v}} + d_{\tilde{v}\tilde{w}} + d_{\tilde{w}\tilde{u}} = 0 \,. \tag{B.2}$$

Furthermore, we get an equation

$$\sum_{\tilde{w} \in \mathcal{N}(\tilde{v})} \lambda_{\tilde{v}\tilde{w}} d_{\tilde{v}\tilde{w}} = 0 \tag{B.3}$$

for each vertex $\tilde{v} \in \tilde{V}$. The three equations (B.1)–(B.3) form a homogeneous linear system of $|\tilde{E}| + |\tilde{\Delta}| + |\tilde{V}|$ equations for the $2|\tilde{E}|$ unknowns $d_{\tilde{v}\tilde{w}}$. The equations (B.1) and (B.2) are linearly dependent, since

$$\sum_{\substack{\tilde{e} \in \tilde{E} \\ \tilde{v}, \tilde{w} \in \tilde{e}}} \underbrace{(d_{\tilde{v}\tilde{w}} + d_{\tilde{w}\tilde{v}})}_{\text{(B.1)}} - \sum_{\substack{\tilde{\delta} \in \tilde{\Delta} \\ \tilde{u}, \tilde{v}, \tilde{w} \in \tilde{\delta}}} \underbrace{(d_{\tilde{u}\tilde{v}} + d_{\tilde{v}\tilde{w}} + d_{\tilde{w}\tilde{u}})}_{\text{(B.2)}} = 0 \,.$$

According to the Euler formula $|\tilde{V}| - |\tilde{E}| + |\tilde{\Delta}| = 2 - 2g = 0$ for the doubly periodic case, the system has at least

$$2|\tilde{E}| - (|\tilde{E}| + |\tilde{\Delta}| + |\tilde{V}|) + 1 = 1$$

non-trivial solutions. The following example shows that no two linearly independent solutions exist in general. *Consequently, doubly periodic generalized plane near-triangulations $\mathcal{G}$ without boundaries do not admit convex combination mappings for general weights.*

Example. We consider the doubly periodic generalized plane near-triangulation shown in Fig. B.12 with $|\tilde{V}| = 9$, $|\tilde{E}| = 27$ and $|\tilde{\Delta}| = 18$. The weights are chosen uniformly, $\lambda_{ij} = \lambda_{ji} = \frac{1}{6}$, except for $\lambda_{12} = \frac{1}{6} + \varepsilon$ and $\lambda_{14} = \frac{1}{6} - \varepsilon$. The system of linear equations (B.1)–(B.3) has rank 53 if $\varepsilon \neq 0$ and 52 otherwise.

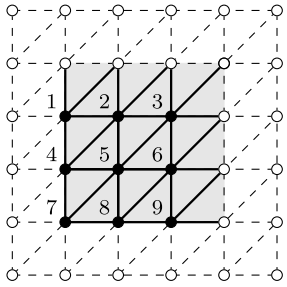

Fig. B.12. An example showing that doubly periodic generalized plane near-triangulations without boundaries do not admit convex combination mappings for general weights. The black dots, solid lines and gray triangles depict the representatives of the vertices, edges and faces with respect to the equivalence relation $\sim$.

For symmetric weights, however, the equations (B.1) and (B.3) are also linearly dependent, since

$$\sum_{\substack{\tilde{e}\in\tilde{E}\\ \tilde{v},\tilde{w}\in\tilde{e}}} \underbrace{(\lambda_{\tilde{v}\tilde{w}} d_{\tilde{v}\tilde{w}} + \lambda_{\tilde{w}\tilde{v}} d_{\tilde{w}\tilde{v}})}_{\text{(B.1)}} - \sum_{\tilde{v}\in\tilde{V}} \underbrace{\sum_{\tilde{w}\in\mathcal{N}(\tilde{v})} \lambda_{\tilde{v}\tilde{w}} d_{\tilde{v}\tilde{w}}}_{\text{(B.3)}} = 0\,,$$

where the equation (B.1) was multiplied by $\lambda_{\tilde{v}\tilde{w}} = \lambda_{\tilde{w}\tilde{v}}$. Therefore, this system has two linearly independent solutions for symmetric weights, hence a convex combination mapping exists in this case. This result extends to the case of quasi-symmetric weights, which take the form $\lambda_{\tilde{v}\tilde{w}} = \varrho_{\tilde{v}}\,\sigma_{\tilde{v}\tilde{w}}$ with certain symmetric pre-weights $\sigma_{\tilde{v}\tilde{w}} = \sigma_{\tilde{w}\tilde{v}}$ and scaling factors $\varrho_{\tilde{v}}$.

References

Aigerman, N., Lipman, Y., 2015. Orbifold Tutte embeddings. ACM Trans. Graph. 34, 190–191.

Bracco, C., Giannelli, C., Großmann, D., Sestini, A., 2018. Adaptive fitting with THB-splines: error analysis and industrial applications. Comput. Aided Geom. Des. 62, 239–252.

Campen, M., Shen, H., Zhou, J., Zorin, D., 2019. Seamless parametrization with arbitrary cones for arbitrary genus. ACM Trans. Graph. 39.

Deng, C., Chang, Q., Hormann, K., 2020. Iterative coordinates. Comput. Aided Geom. Des. 79, 101861.

DeRose, T., Meyer, M., 2006. Harmonic Coordinates, Pixar Technical Memo 06-02, Pixar Animation Studios.

Floater, M., 1997. Parametrization and smooth approximation of surface triangulations. Comput. Aided Geom. Des. 14, 231–250.

Floater, M., 2003. One-to-one piecewise linear mappings over triangulations. Math. Comput. 72, 685–696.

Floater, M., Hormann, K., 2005. Surface parameterization: a tutorial and survey. In: Advances in Multiresolution for Geometric Modelling. Springer, pp. 157–186.

Floater, M.S., Pham-Trong, V., 2006. Convex combination maps over triangulations, tilings, and tetrahedral meshes. Adv. Comput. Math. 25, 347–356.

Gortler, S.J., Gotsman, C., Thurston, D., 2006. Discrete one-forms on meshes and applications to 3D mesh parameterization. Comput. Aided Geom. Des. 23, 83–112.

Gotsman, C., Gu, X., Sheffer, A., 2003. Fundamentals of spherical parameterization for 3D meshes. ACM Trans. Graph. 22, 358–363.

Gu, X., Yau, S.T., 2003. Global conformal surface parameterization. In: Proc. Symposium on Geometry Processing, Eurographics, pp. 127–137.

Hochberg, R., McDiarmid, C., Saks, M., 1995. On the bandwidth of triangulated triangles. Discrete Math. 138, 261–265.

Hoschek, J., Lasser, D., 1993. Fundamentals of Computer Aided Geometric Design. AK Peters.

Jiang, Z., Schneider, T., Zorin, D., Panozzo, D., 2020. Bijective projection in a shell. ACM Trans. Graph. 39, 247.

Jüttler, B., Langer, U., Mantzaflaris, A., Moore, S.E., Zulehner, W., 2014. Geometry + simulation modules: implementing isogeometric analysis. Proc. Appl. Math. Mech. 14, 961–962.

Richter-Gebert, J., 1996. Realization Spaces of Polytopes. Lecture Notes in Math., vol. 1643. Springer, Berlin Heidelberg.

Saboret, L., Alliez, P., Lévy, B., Rouxel-Labbé, M., Fabri, A., 2019. Triangulated surface mesh parameterization. CGAL User and Reference Manual 4.14 Edition. CGAL Editorial Board.

Shivakumar, P., Chew, K.H., 1974. A sufficient condition for nonvanishing of determinants. Proc. Am. Math. Soc. 43, 63–66.

Taussky, O., 1949. A recurring theorem on determinants. Am. Math. Mon. 56, 672–676.

Tong, Y., Alliez, P., Cohen-Steiner, D., Desbrun, M., 2006. Designing quadrangulations with discrete harmonic forms. In: Sheffer, A., Polthier, K. (Eds.), Symposium on Geometry Processing, Eurographics, pp. 201–210.

Tutte, W.T., 1963. How to draw a graph. Proc. Lond. Math. Soc. 3, 743–767.

Vaitkus, M., Várady, T., 2018. Parameterizing and extending trimmed regions for tensor-product surface fitting. Comput. Aided Des. 104, 125–140.

Weiss, V., Andor, L., Renner, G., Várady, T., 2002. Advanced surface fitting techniques. Comput. Aided Geom. Des. 19, 19–42.